Advanced Steel Construction – Vol. 20 No. 3 (2024) 241–252
DOI:10.18057/IJASC.2024.20.3.4

RESEARCH ON BENDING PERFORMANCE AND BILINEAR MODEL OF AN IMPROVED BOLT-COLUMN (BC) JOINT

Zhi-Cheng Xiao, Ren Li, Hui-Jun Li *, Guang-Hong Luo and Bao-Hui Li

College of Water Resources and Architectural Engineering, Northwest A&F University, Yangling 712100, Shaanxi, China
** (Corresponding author: E-mail: lihuijun2893118@163.com)*

ABSTRACT

The semi-rigid bolt-column (BC) joint, which is a component of large-span single-layer reticulated structures, demonstrates a considerable application potential. In this study, the BC joint is innovatively modified using two flanges, one web and two additional high-strength bolts. The comparative analysis between the original and improved joints reveals a notable enhancement in bending performance, including 62.59% increase in initial rotational stiffness, 116.82% increase in initial yield moment, and 87.57% increase in ultimate moment. Subsequently, a total of 66 finite element (FE) models of the improved BC joint, incorporating varying parameters such as bolt diameter, bolts' vertical distance, flange thickness, front plate thickness, and column node thickness, are conducted to systematically evaluate its bending performance. Furthermore, the effect of axial force on the bending performance is discussed. Finally, a bilinear model is developed to predict the moment-rotation relationships of improved BC joint.

ARTICLE HISTORY

Received: 13 January 2024
Revised: 18 February 2024
Accepted: 20 February 2024

KEYWORDS

Improved BC joint;
Parametric analysis;
Bending performance;
Failure mode;
Bilinear model

1. Introduction

The reticulated shell, a common form of large-span structures, is widely applied in large public buildings such as terminals, stadiums and exhibition halls. However, the application of assembled reticulated shells is limited in engineering due to the assumption of ideal hinges for assembled joints despite their advantages including convenient and high-precision construction and reasonable force. In reality, most of the joints exhibit bending performance and semi-rigid features.

As research progresses, an increasing number of scholars have discovered the semi-rigid behavior of assembled joints. Ma *et al* [1-2] and Fan *et al* [3] introduced a new type of semi-rigid connection known as the bolt-column joint, enabling efficient connections with members of H, I, and rectangular section. A series of experimental and numerical tests were conducted by Ma [1-2] to investigate the impact of geometric parameters on the mechanical performance of the joint. Based on Eurocode 3 (EC3) component method, a trilinear mathematical model was developed for predicting its the moment-rotation relationship. Fan [3] utilized optimization analysis in FE models to determine the rotational dimensions of BC joint components, following the principle of 'strong connection and weak plate. However, the BC joint proposed by them, despite its merits, exhibits structural deficiencies in cone head design. The limited bending performance of this joint may constrain its application.

In addition, Han *et al* [4] proposed both theoretical and practical equations to calculate the initial stiffness of welded hollow spherical joints, while also presented a mechanical model that considers the joint's stiffness characteristics. Comparison with experimental results showed an average difference of 8% for the mechanical model's prediction of the load-rotation curve's initial slope, and an average error of 7% for estimating the ultimate bearing capacity. Yan *et al* [5] presented a comprehensive investigation of the welding process involved in connecting hollow spherical joints to pipes, with a specific focus on the welds. This study included an analysis and summary of the distribution pattern and specific mode of residual stress in these joints, while also parametrically investigating how variations in joint configuration dimensions impact the distribution of welding residual stress. Mashrah *et al* [6] proposed two novel types of socket joints: a steel dovetail joint without teeth pattern and a steel dovetail joint with teeth pattern. Experimental and numerical tests were conducted to investigate the bearing capacities and failure modes of these new joint systems under axial tensile loads. According to Fan *et al* [7-8], numerical simulations can provide valuable technical guidance for the design and application of bolt-ball joints and other semi-rigid joints, through comparison between a three-dimensional solid model generated using the ANSYS package and experimental results. Additionally, tests were conducted to examine the mechanical behavior of socket joints and bolt-ball joints. The findings indicated that the initial bending stiffness of these joints is influenced by axial compressive force, while its impact on the bending moment capacity varies across different joint types. Yu *et al* [9] investigated the impact of different parameters related to the bolt-ball joint, such as bolt size, initial tightening force, thickness of cone tail wall and sleeve, on its ability to withstand bending; also the study developed a power function model to establish the relationship between moment and rotation for the bolt-ball joint. Xue *et al* [10] investigated the bending performance of the threaded-sleeve connection through experimental methods and finite element models; additionally, this study proposed a mechanical model based on the Kishi-Chen power model to predict its moment-rotation behavior. Ma *et al* [11] demonstrated the impact of joint stiffness on the seismic behavior of semi-rigid single-layer reticulated shell structures, considering both initial imperfections and progressive material degradation. Shan [12] investigated the failure modes and maximum load-bearing capacities of hub-shaped inlay joints under different loading conditions, confirming that the minimum cross-section could serve as a suitable substitute for determining their load-bearing capacities. Han *et al* [13] have proposed a novel Assembled Hub (AH) joint that incorporates two unique connection types, and also presented theoretical solutions for the elastic stiffness and bearing capacity of this innovative joint system using the component method. Zhang *et al* [14] investigated the impact of size parameters on the bending stiffness and torsional stiffness of hub-shaped inlay joints. The failure mechanisms of the joint were examined under various stiffness conditions, and a moment-rotation relationship model for the joint was derived using regression analysis. Golea *et al* [15] introduced a novel analytical approach utilizing the component method, which was verified by conducting five physical experiments. By incorporating additional analytical equations to characterize fundamental elements of steel joints, this proposed approach expanded the scope of the component method to encompass strain-hardening and ductility considerations in components. The conventional aluminum alloy Temcor joint was enhanced by Ma *et al* [16-18] through the incorporation of a central hollow hexagonal prism and several front bolts. The study utilized FE models to explore the optimal parameters of the joint, taking into account factors such as the number and placement of front bolts, bolt-hole deviation, pretension force in bolts, thickness of the front plate, and heat-affected zone resulting from welding operations. Feng *et al* [19] presented a novel type of bolted connection known as the Ring-sleeve joint, which was specifically developed for single-layer reticulated shells. To investigate the mechanical characteristics of this joint, prototype static experiments and numerical analyses were conducted under various load conditions such as bending moment, shear force, and axial force. The results indicated that the joints exhibited three different failure modes depending on the ratio between bolt bearing capacity and tube bearing capacity. An advanced form of the Aluminum Alloy Temcor joint system, referred to as the Aluminum Alloy Penetrating joint, was introduced by Ma *et al* [20]; and the joint's resistance to rotation was evaluated through an out-of-plane static flexural test. Moreover, the mechanical behavior of T-stub aluminum joints [21-22], MERO ball joints [23-24], aluminum alloy gusset joints [25], and K-joints made from CHS aluminum profiles [26] has been comprehensively investigated in previous studies.

To enhance the bending performance of the BC joint, a novel cone structure is incorporated into the joint design. Firstly, the FE model of BC joint is validated using an existing model. Then the bending performance between the BC joint and the improved one is compared. Secondly, a parametrical study is

conducted to elucidate the general law of the improved BC joint's bending performance. Its moment-rotation curves and failure modes are obtained and discussed. Finally, a bilinear model of the moment-rotation relationship is developed and validated.

2. The modeling and verification of BC joints

2.1. Modeling

The BC joint is comprised of a hollow column node, a cone component, and two bolts with high strength, in which the cone consists of five components: a front plate, a middle plate, two side plates, and an end plate. The configuration of BC joint is depicted in Fig. 1. In this paper, the BC joint connecting rectangular member is simulated with C3D8R solid element in ABAQUS software package. The analysis of a single bar is conducted based on the structural symmetry and load conditions, as depicted in Fig. 2. In terms of material properties, Q235 steel is used for the cone part and member, while 40Cr steel and 45Mn steel is employed for high-strength bolts and column node respectively, as listed in Table 1. The contact pairs in the setting are defined as follows [1]: binding ties are applied to the surface between bolts and column node, self-contact is considered between bolts and front plate, while surface-to-surface contact is utilized for all other interfaces. As for contact properties, normal direction employs hard contact and tangent direction adopts Coulomb friction with a coefficient of 0.3. The loading surface is selected to be the end face of the member and fixed constraint is used for the cross section of the column node in order to prevent rigid body displacement during the analysis process.

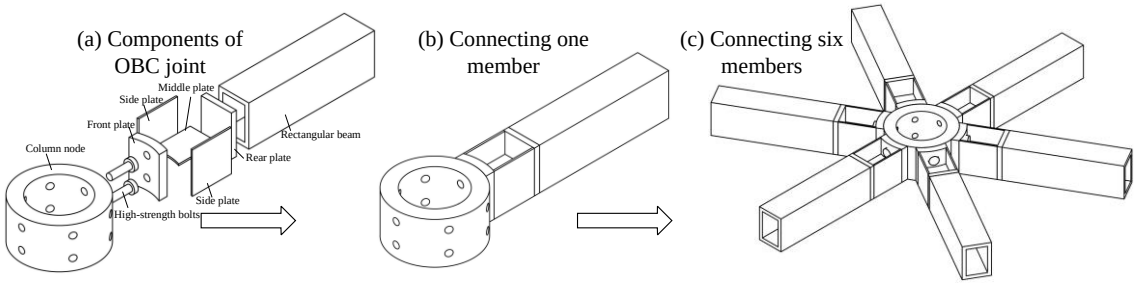

Fig. 1 The configuration of BC joint

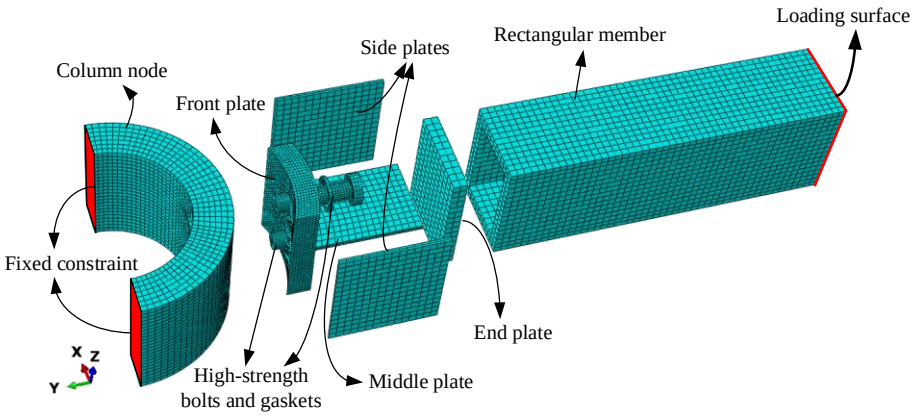

Fig. 2 The FE model of BC joint

Table 1
Material properties of components [1-3]

Components	Material	Yield strength $f_y\left(\mathrm{N/mm^2}\right)$	Tensile strength $f_u\left(\mathrm{N/mm^2}\right)$	Young's modulus $E\left(\mathrm{N/mm^2}\right)$	Poisson's ratio μ
Side and middle plates	Q235 steel	304	456	207848	0.33
Front and end plates		235	235	210000	0.33
beam		269	407	205569	0.33
Bolts and gaskets	40Cr steel	975	1171	213302	0.33
Column node	45Mn steel	355	355	210000	0.29

2.2. Verification

In order to verify the reliability of numerical tests in this paper, FE model is established based on the specific specimen sizes and loading conditions from previous tests and numerical models from Ma *et al* [1-2] and Fan *et al* [3]. The dimensions of the components are specified as follows: the column node has an outer radius 150mm with a thickness of 50mm; the front plate is 30mm thick and the rear plate is 20mm thick; the side plates and middle plate both have a thickness of 6mm; bolts with a diameter of 24mm are spaced at vertical interval of 78mm and subjected to a pre-tightening force of 225 kN. Additionally, load is applied at the member's end.

The bending moment-rotation curve of the BC joint is depicted in Fig. 3, illustrating its main features such as initial rotational stiffness (S_i), initial yield moment (M_{inf}) and ultimate moment (M_u). Once M_{inf} is reached, the joint transitions into the plastic yield phase; when reaching M_u , failure is deemed to occur. Moreover, the moment and rotation are exerted from the section between rear plate and member.

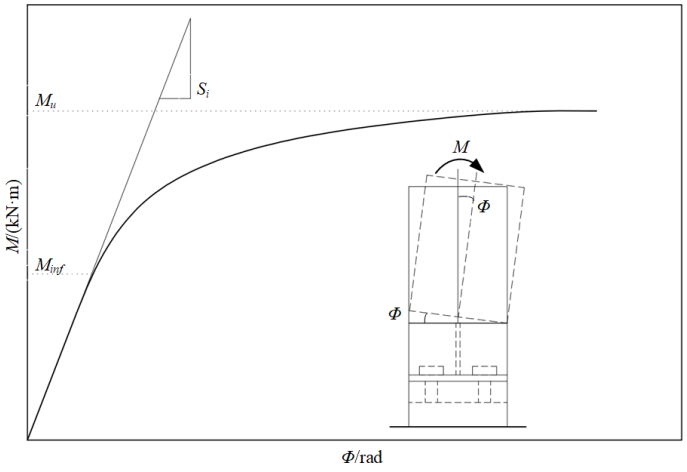

Fig. 3 Main features of the *M*-Φ curve

The bending moment-rotation curve from Ref. [1] and numerical result obtained in this study are compared in Fig. 4. The main indexes of these curves are shown in Table 2. It can be observed that the moment-rotation curve from the FE model is in good agreement with the one from Ref. [1] in the inelastic stage, but exhibits a slight deviation in the elastic stage. The initial stiffness, initial moment and ultimate moment deviates by 7.06%, 1.93% and 0.92% respectively, all within an error margin below 10%. It can be seen that the FE model in this paper exhibits effectiveness in representing the real bending behavior of the BC joint.

3. Development of improved BC joint and comparison on original BC joint

3.1. The improved BC joint

The Mises stress contour diagram in Fig. 4 reveals that BC joint fails due to the formation of plastic hinge in side plates, which precedes the yield failure of bolts; additionally, a significant yield area is observed in side plates and a small one is seen in bolts, indicating the underutilization of the material properties of bolts. These findings reveal the deficiencies in current dimensions and structural arrangement of BC joint.

To enhance the bending performance of BC joint, modifications are made by the removal of side plates and middle plate and the addition of flanges and web, namely rotating the cone part of BC joint. Furthermore, two additional bolts are included to ensure superior mechanical performance in cases where joint failure occurs due to bolt damage. Based on the material properties and contact pairs in Section 2.1, the finite element model of improved BC joint is established in ABAQUS package, as shown in Fig. 5.

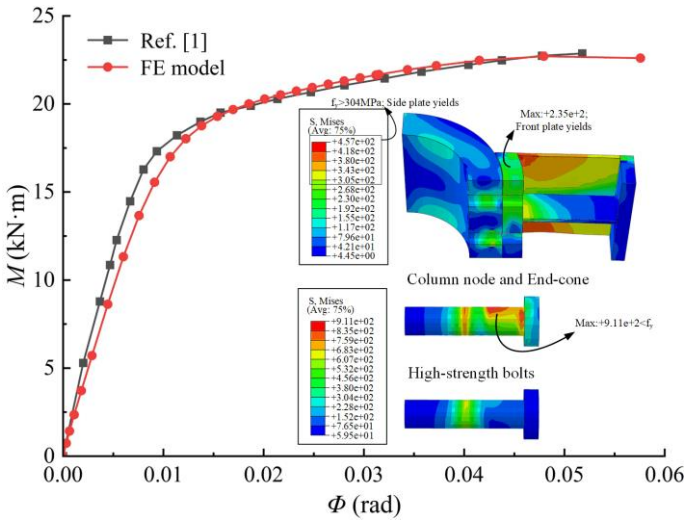

Fig. 4 Moment-rotation curves comparison between Ref. [1] and FE model in this study

Table 2
Main indexes of bending moment-rotation curves of Ref. [1] and FE model

Model	S_i (kN·m/rad)	M_{inf} (kN·m)	M_u (kN·m)
Ref. [1]	2062.86	8.79	22.81
FE model	1917.19	8.62	22.60

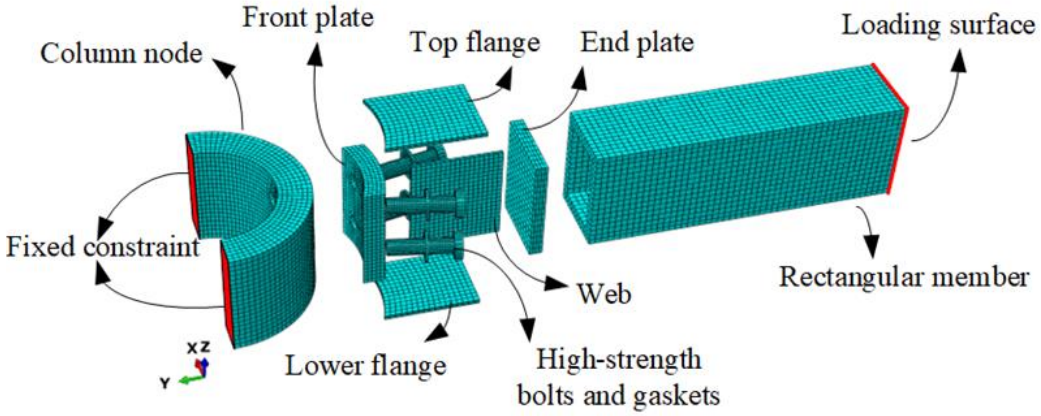

Fig. 5 Arrangement of the improved BC joint

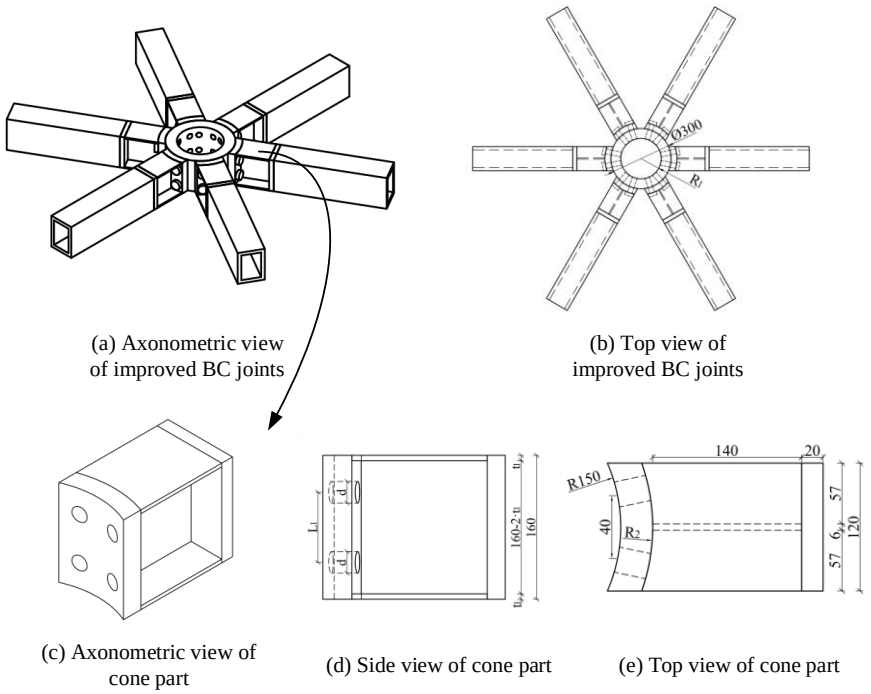

Fig. 6 Detailed dimensions of improved BC joint

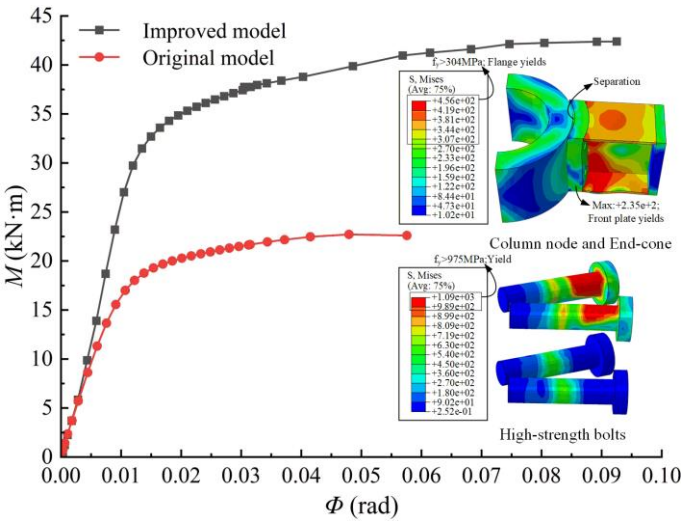

Fig. 7 Moment-rotation curves of the improved and the original BC joints

3.2. Comparative analysis of bending performance between the improved and the original BC joints

To compare the bending performance of the improved BC joint with the original one, a numerical model of the improved BC joint with dimensions and loading condition of Section 2.2 is established. The specific parameters of the joint are as follows: flange thickness is 6mm; inner diameter of column node is 100mm; outer diameter of front plate is 180mm; bolt diameter is 24mm; vertical distance between bolts is 78mm. The pre-tightening force of bolts is taken as 225kN and other parameters are shown in Fig.6.

The moment-rotation curves of BC joint and improved BC joint, and the stress distribution of the column node, cone part and bolts of the improved BC joint are shown in Fig. 7. It can be observed that the improved model exhibits a substantial enhancement in initial bending stiffness, initial moment and ultimate moment compared to the original model.

Careful examination for stress contour diagram reveals minor separation between the column node and the cone part, remarkable yield and deformation of the flanges and notable increase in stress distribution within the bolts. It indicates that the novel designed structure demonstrates superior utilization in material properties. In addition, Table 3 lists the key joint bending indexes of both the joints, it can be seen that improved BC joint exhibits 62.59% increase in initial rotational stiffness, 116.82% increase in initial yield moment, and 87.57% increase in ultimate moment.

Table 3
Main indexes of bending performance of the original and improved models

Model	$S_i\,(\mathrm{kN\cdot m/rad})$	$M_{inf}\,(\mathrm{kN\cdot m})$	$M_u\,(\mathrm{kN\cdot m})$
Original model	1917.19	8.62	22.60
Improved model	3117.11	18.69	42.39

4. Parametric study on bending performance of improved BC joint

In present section, the numerical models of the improved BC joint are used for parametric studies, taking into account bolt diameter, bolts' vertical distance and flange thickness, front plate thickness and column node thickness. The specific geometric dimensions are shown in Table 4. Additionally, the effect of axial force on the bending performance of improved BC joint is discussed in the end of this section.

Table 4
Detailed dimensions of the numerical models

Beam section (mm)	Bolt diameter $d\ (\mathrm{mm})$	Vertical distance of bolts $L_1(\mathrm{mm})$	Flange thickness $t_1(\mathrm{mm})$	Front plate thickness $t_2(\mathrm{mm})$	Column node thickness $t_3(\mathrm{mm})$
□160×120×16×16	21,24,27,30	78	6,8,10,12,14,16	30	50
□160×120×16×16	24	72,78,84	6,8,10,12,14,16	30	50
□160×120×16×16	24	78	6,8,10,12,14,16	20,25,30,35	50
□160×120×16×16	24	78	6,8,10,12,14,16	30	30,40,50

4.1. Effect of bolt diameter and flange thickness on the bending performance of the improved BC joint

The moment-rotation curves and stress distribution of joints with bolt diameter 21, 24, 27 and 30mm, and flange thickness 6, 8, 10, 12, 14 and 16mm are depicted in Figs. 8-9. The influence of bolt diameter and flange thickness on the bending performance of joints is analyzed specifically.

The observation reveals that, with a constant bolt diameter and an increasing flange thickness, the ultimate moment of joints exhibits a significant increase with a gradually diminishing rate, while its initial bending stiffness demonstrates a slight enhancement. Additionally, as the flange thickness increases, there is continuous development in terms of the yield area and deformation of bolts, as well as the separation between the cone part and column node.

Taking the joints with bolt diameter of 21mm as an example, the failure modes of improved BC joint is discussed as follows. When $t_1 \le 8\mathrm{mm}$, severe deformation occurs in both front plate and flanges before separation occurrence between cone part and column node is clear. The plastic hinge formation during first half of cone part results the failure of joints. When $8\mathrm{mm} < t_1 \le 12\mathrm{mm}$, front plate and compression flange still experience significant damage and the separation between front plate and column node is apparent, which means tensile bolt's surface deformation greatly increases. Hence, joints fail due to simultaneous yielding among front plate, flanges and bolts. When $t_1 > 12\mathrm{mm}$, the deformation of flanges is small, and the joints damage attributed to the tensile failure of bolts.

The Mises stress contour diagrams of joints with different bolt diameters show that the yield area of front plate decreases gradually by increasing bolt diameter. It can be attributed to the fact that bolts share more bending moment, and the bending performance of flanges is made better use of. In the case where flange thickness (such as $t_1 = 8\mathrm{mm}$ and $t_1 = 12\mathrm{mm}$) remains constant, as the bolt diameter increases, so does the ultimate moment. However, when $d > 27\mathrm{mm}$, bolt diameter affects the moment-rotation curves slightly.

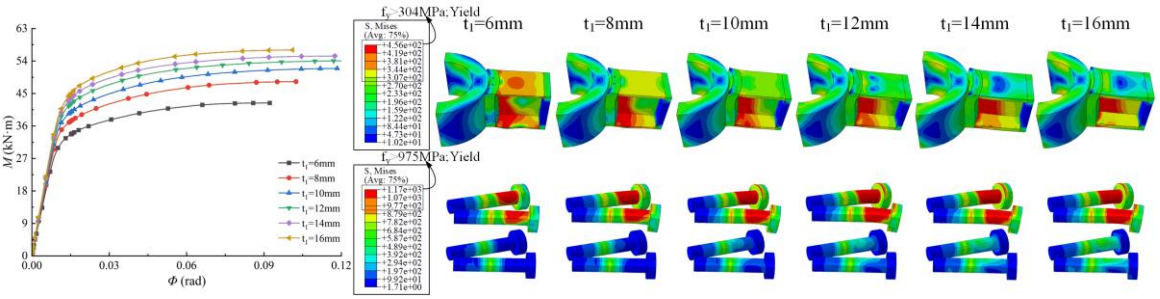

(a) Bolt diameter 21mm

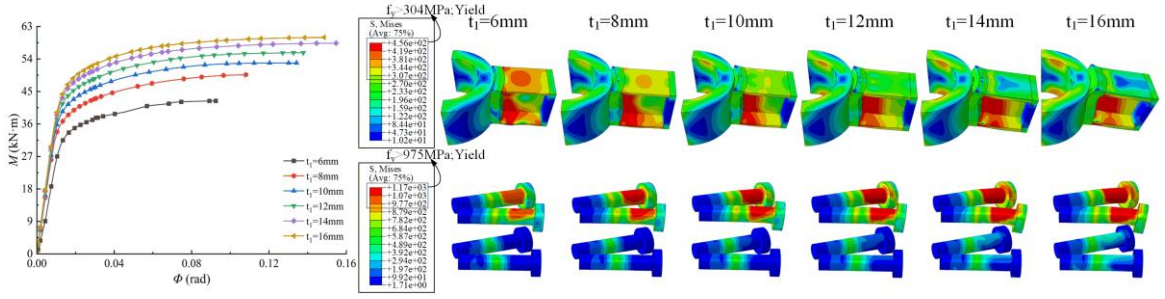

(b) Bolt diameter 24mm

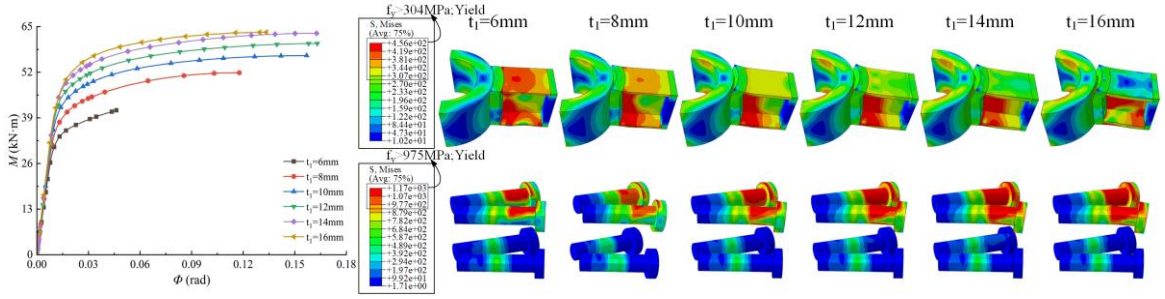

(c) Bolt diameter 27mm

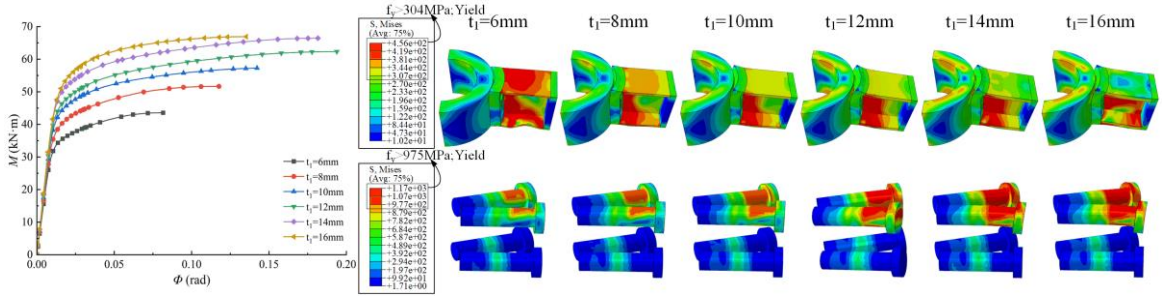

(d) Bolt diameter 30mm

Fig. 8 Moment-rotation curves and stress distribution of joints with different bolt diameters and flange thicknesses

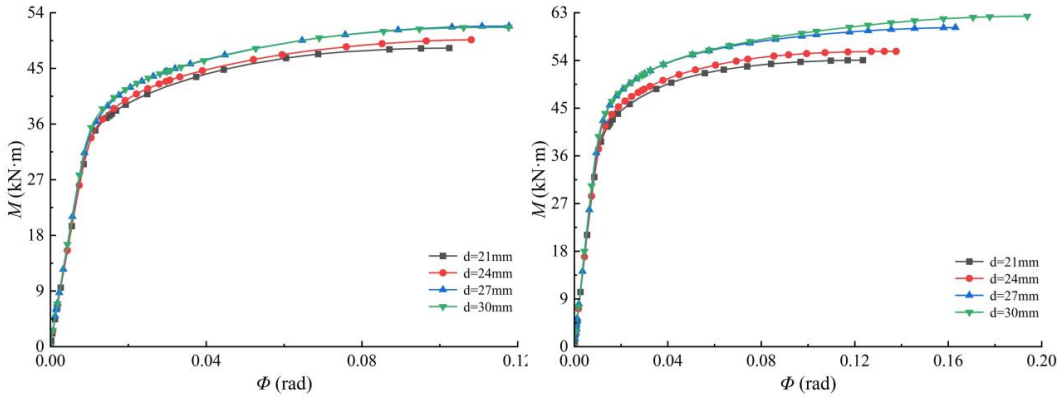

(a) t_l=8mm (b) t_l=12mm

Fig. 9 Moment-rotation curves with flange thicknesses of 8mm and 12mm and different bolt diameters

4.2. Effect of vertical bolt spacing and flange thickness on the bending performance of the improved BC joint

For the improved BC joint, three bolts' vertical distances, 72, 78 and 84mm, and six flange thicknesses, 6, 8, 10, 12, 14 and 16mm, are considered in the examination. Figs. 10-11 show the moment-rotation response and stress distribution at the column node, cone part and bolts of joints. It can be concluded that the general law of change in the moment-rotation curve and stress distribution of joints is similar to the Section 4.1 by increasing flange thickness.

From the stress distribution of joints, it can be observed that the stress reduction occurs in bolts with increasing vertical distance of bolts; meanwhile the separation between column node and front plate narrows. It indicates that increasing vertical distance of bolts can enhanced the bending performance of joints. Furthermore, as flange thickness (take $t_1 = 8\text{mm}$ and $t_1 = 12\text{mm}$ as examples) stay the same, by increasing bolts' vertical distance, the ultimate moment enhances stably; however, it exhibits little influence on initial bending stiffness.

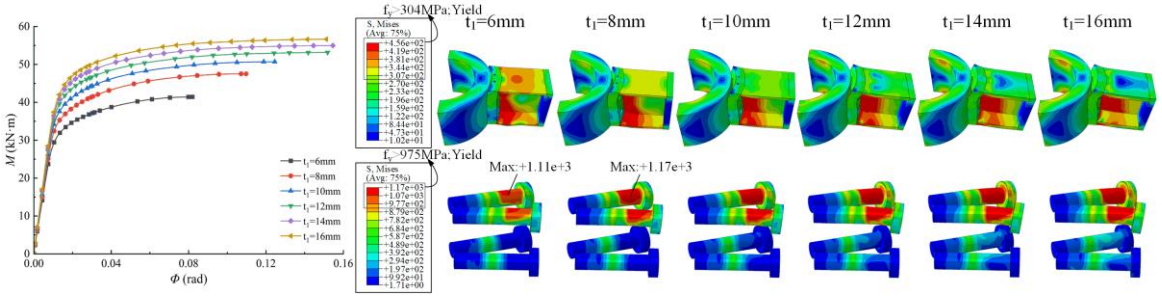

(a) Bolts' vertical distance 72mm

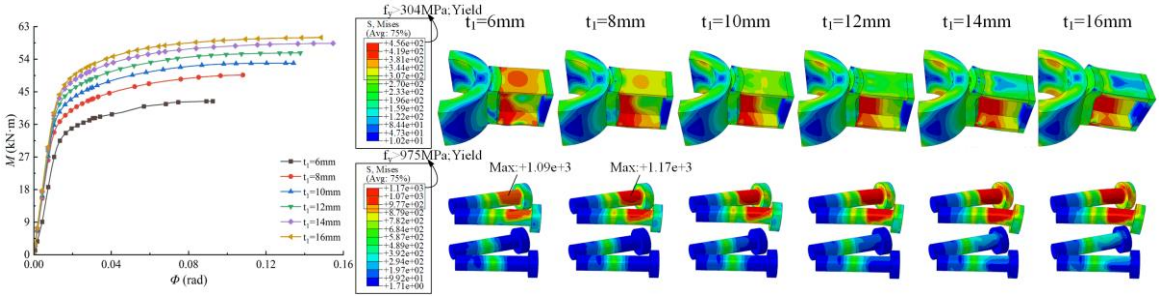

(b) Bolts' vertical distance 78mm

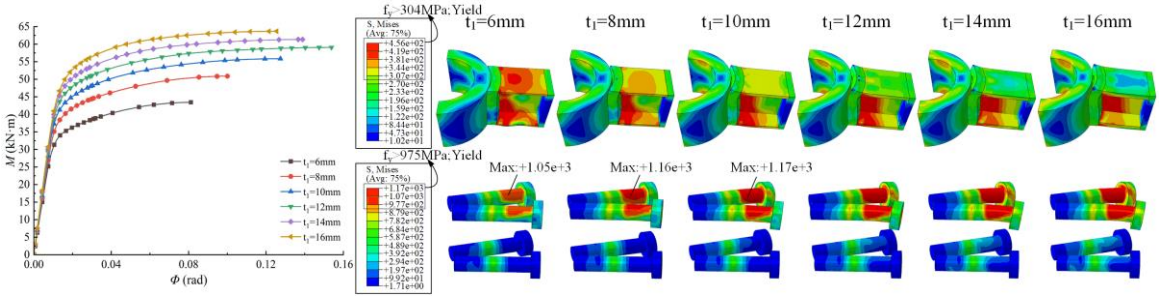

(c) Bolts' vertical distance 84mm

Fig. 10 Moment-rotation curves and stress distribution of joints with different bolts' vertical distances and flange thicknesses

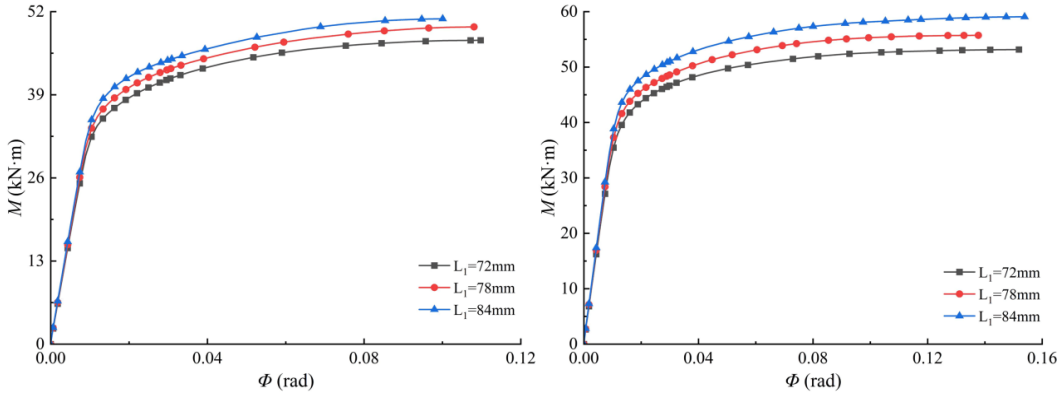

(a) t_1=8mm (b) t_1=12mm

Fig. 11 Moment-rotation curves with flange thicknesses of 8mm and 12mm and different vertical distances of bolts

4.3. Effect of thicknesses of front plate and flange on the bending performance of the improved BC joint

The front plate thickness of 20, 25, 30 and 35mm and the flange thickness of 6, 8, 10, 12, 14 and 16mm are considered in numerical models. Moment-rotation curves and stress distribution of joints are shown in Figs. 12-13. In the figures, the bending performance increases significantly with increasing flange thickness while keeping a constant thickness of front plate. However, when $t_2 \geq 25\text{mm}$, the flange with thickness over 14mm makes a small influence on the curve. Beyond that, the change rule of stress variation of joints is similar to Section 4.1.

Contrasting the stress distribution of the joints with different thicknesses of front plate, it can be observed that the stress and deformation of flanges increase significantly with an increasing thickness of the front plate, and the separation between column node and cone part decreases noticeably. The stress on bolts increases with a thicker front plate when $t_2 \leq 30\text{mm}$, but it decreases when $t_2 > 30\text{mm}$. Plastic hinge of the flanges is the main failure mode for the joints with front plate thickness of 35mm, except for joints with flange thickness of 16mm. What's more, when flange thickness (for example, $t_1 = 8\text{mm}$ and $t_1 = 12\text{mm}$) is unchanged, the ultimate moment of joint increases apparently and there is a great improvement when $t_2 > 30\text{mm}$.

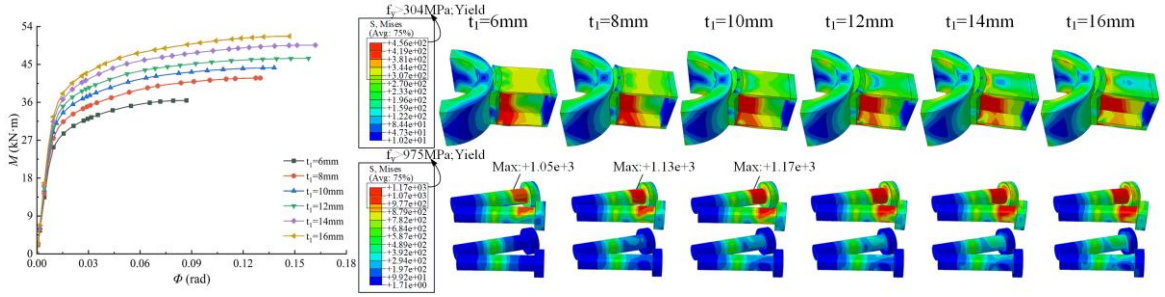

(a) Front plate thickness of 20mm

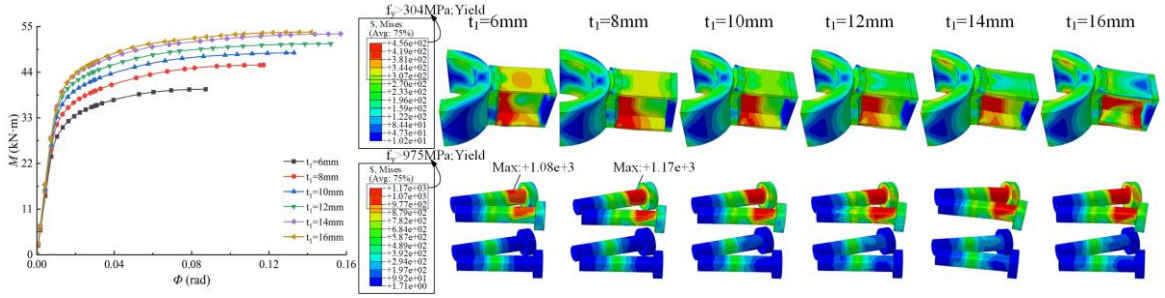

(b) Front plate thickness of 25mm

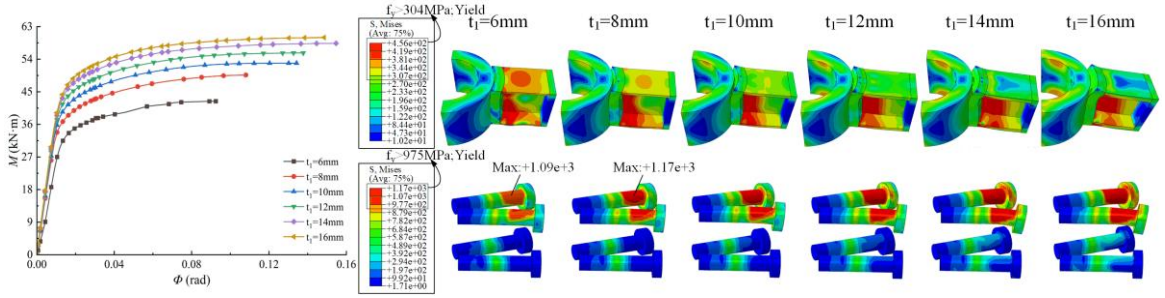

(c) Front plate thickness of 30mm

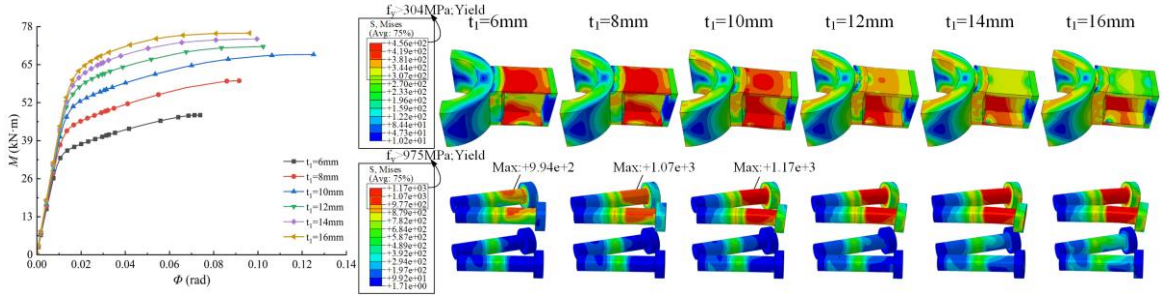

(d) Front plate thickness of 35mm

Fig. 12 Moment-rotation curves and stress distribution of joints with different front plate's and flange's thicknesses

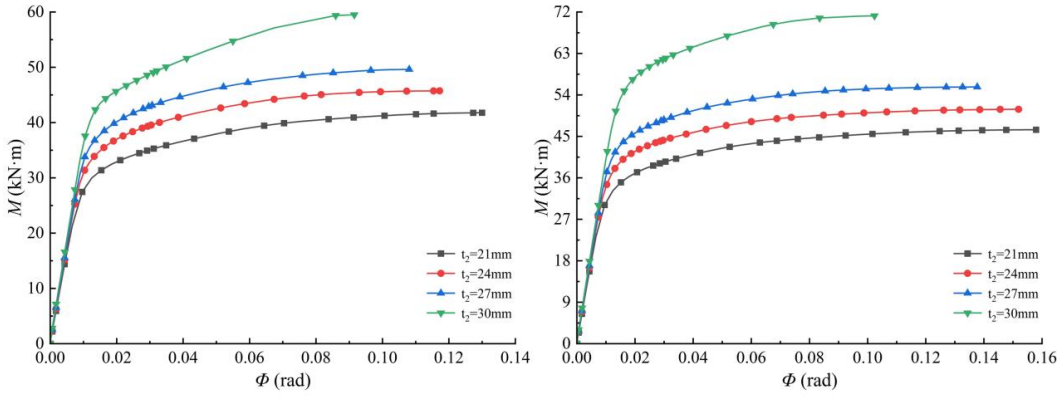

(a) t_l=8mm (b) t_l=12mm

Fig. 13 Moment-rotation curves with flange thicknesses of 8mm and 12mm and different thicknesses of front plate

4.4. Effect of thicknesses of column node and flange on the bending performance of the improved BC joint

In this section, three column node thicknesses (30, 40 and 50mm) and six flange thicknesses (6, 8, 10, 12, 14 and 16mm) are taken into account. Moment-rotation curves and Mises stress contour diagrams are as shown in Figs. 14-15, it can be seen that when $t_3 \geq 40\text{mm}$, by increasing flange thickness, the change law in moment-rotation curves and stress variation is similar to Section 4.1. However, the law differs when $t_3 < 40\text{mm}$. In this condition, flanges with thickness over 10mm affect the moment-rotation curve slightly; moreover, careful observation for the stress distribution of joints reveals that the failure modes of joints are the same as $t_1 > 8\text{mm}$: a large area of column node yields, resulting in a plastic hinge and then joint fails. The stress of bolts decreases for the reason that the formation of plastic hinge in column node occurs before full utilization of bolts. Therefore, column node with a thickness less than 40mm should be avoided. Additionally, by increasing the thickness of column node, little change occurs in the moment-rotation curve and stress distribution of joints, except for joints with column node thickness of 30mm, as shown in Fig. 15.

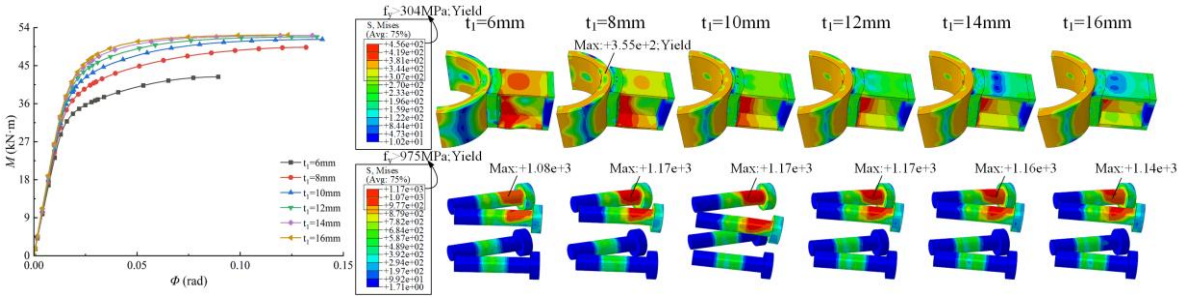

(a) Column node thickness 30mm

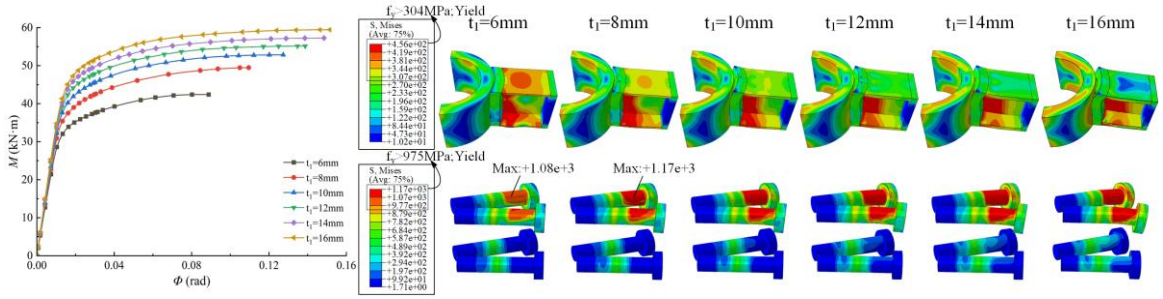

(b) Column node thickness 40mm

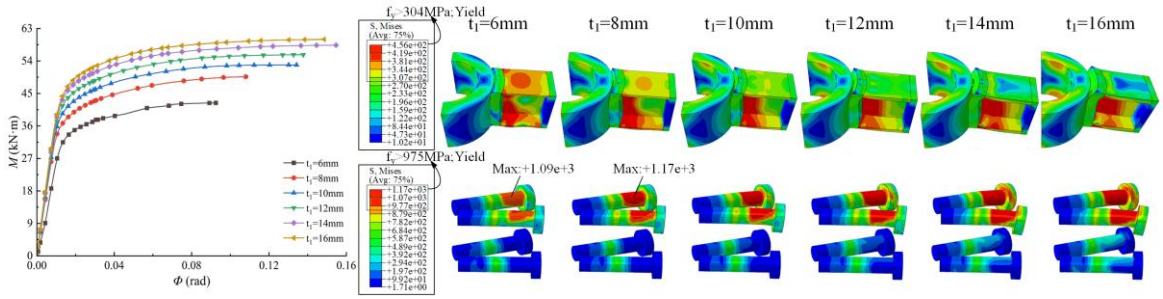

(c) Column node thickness 50mm

Fig. 14 Moment-rotation curves and stress distribution of joints with different column node's and flange's thicknesses

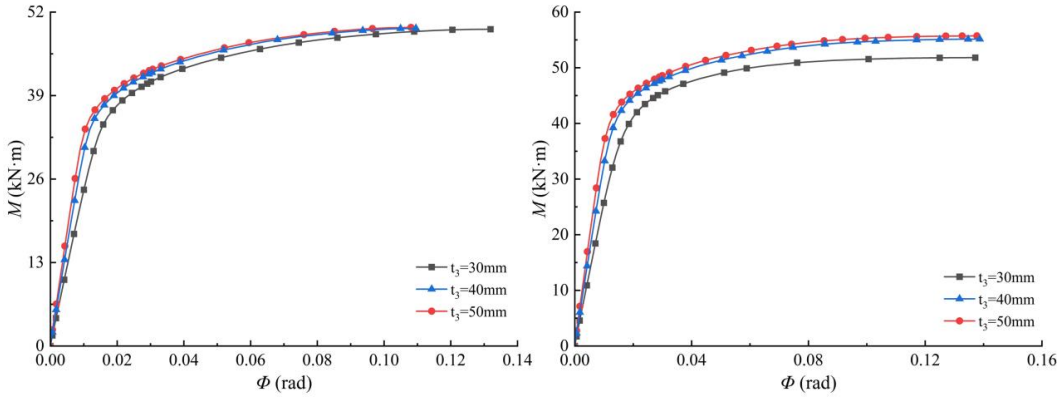

(a) t_1=8mm (b) t_1=12mm

Fig. 15 Moment-rotation curves with flange thicknesses of 8mm and 12mm and different thicknesses of column node

4.5. Effect of axial force on bending performance of the improved BC joint

Taking improved BC joint with d=24mm, L_1=78mm, t_1=10mm, t_2=30mm and t_3=50mm as instance, the effect of axial force on its bending performance is discussed in present section. The characteristics for the bending performance of improved BC joint with prescribed axial force is illustrated in Fig. 16. In the figure, η_c represents the ratio of the prescribed axial compression to the ultimate axial compression of joint; η_t represents the ratio of the prescribed axial tension to the ultimate axial tension of joint. Through numerical axial force

tests on improved BC joint, the values of ultimate axial force are obtained: the ultimate axial compression is 1213.23 kN and the ultimate axial tension is 1277.57 kN. In addition, $K^{\eta_t}_{(j,ini)}/K^{0}_{(j,ini)}$ ($K^{\eta_c}_{(j,ini)}/K^{0}_{(j,ini)}$) represents the ratio of initial stiffness of joints subjected to prescribed tension (compression) to that of joints without prescribed tension (compression); $M^{\eta_t}_u/M^0_u$ ($M^{\eta_c}_u/M^0_u$) represents the ratio of ultimate bending moment of joints subjected to prescribed tension (compression) to that of joints without prescribed tension (compression).

The observation of this figure demonstrates that the axial compression exhibits positive effect on the bending performance when $\eta_c \le 0.3$, while it reveals negative effect when $\eta_c > 0.3$. When $\eta_c \le 0.7$, a significant enhancement occurs in the initial bending stiffness, while the initial elastic stage of the joint exhibits obvious decrease. In addition, with increasing η_c, the stress of both bolts and tensile flange shows remarkable decline, while the compressive flange exhibits the opposite trend.

For joints with prescribed tension, it demonstrates stable decline in bending performance as η_t increasing; in addition, an increasing deformation is observed from the tensile bolts and tensile flange when joint reaches its ultimate moment.

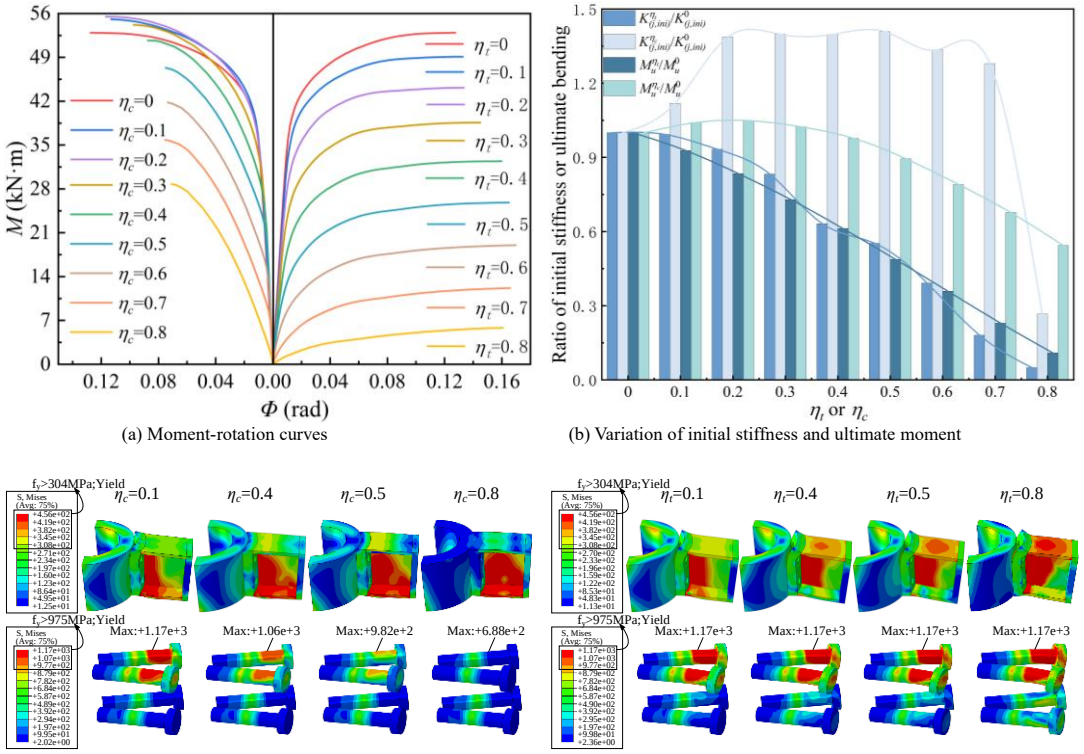

(a) Moment-rotation curves

(b) Variation of initial stiffness and ultimate moment

(c) Mises stress contour diagrams at ultimate moment. (Unit: MPa)

Fig. 16 Characteristics for bending performance of improved BC joint with a prescribed axial force

5. Bilinear model of improved BC joint

5.1. Establishment method of bilinear model

Analyzed as before, the moment-rotation curve of the improved BC joint has obvious feature of bilinear model, which is mainly affected by bolt diameter, vertical distance of bolts, flange thickness and front plate thickness. As shown in Fig. 17 [14], assuming that there is a yield moment $M_s = aM_u$ (a is yield coefficient and M_u is ultimate moment), a can be calculated through energy equivalence method, namely that the area enclosed by moment-rotation curve is equivalent to the one by bilinear model. In addition, S_j represents initial bending stiffness and φ_u represents the rotation corresponding to ultimate moment.

Based on the FE models in Section 4, the bilinear model characteristics (a, φ_u, S_j and M_u) of improved BC joint are obtained and listed in Table 5. From the values of S_j and M_u in the table, it can be seen that the improved BC joint is a typical semi-rigid joint.

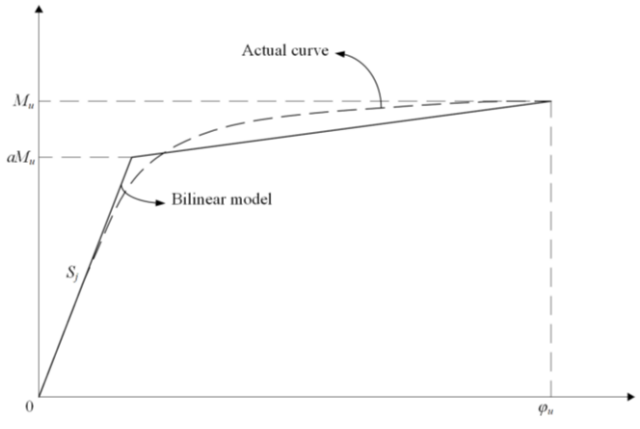

Fig. 17 Bilinear model

Table 5
Bilinear model characteristics of improved BC joint

d(mm)	L_1(mm)	t_1(mm)	t_2(mm)	a	φ_u(rad)	S_j(kN·m/rad)	M_u(kN)
21	78	6	30	0.859	0.092214	3545.33	42.37
21	78	8	30	0.856	0.102434	3689.27	48.29
21	78	10	30	0.865	0.118382	3841.79	51.94
21	78	12	30	0.883	0.123509	3997.48	54.06
21	78	14	30	0.888	0.117440	4103.98	55.39
21	78	16	30	0.875	0.101047	4202.85	57.06

24	78	6	30	0.867	0.092504	2513.08	42.39
24	78	8	30	0.856	0.108057	3510.78	49.62
24	78	10	30	0.891	0.134250	3680.57	52.90
24	78	12	30	0.892	0.137729	3836.38	55.72
24	78	14	30	0.899	0.154670	3961.81	58.38
24	78	16	30	0.900	0.148507	4033.45	59.98
27	78	6	30	0.828	0.046217	3391.20	41.17
27	78	8	30	0.860	0.117756	3644.73	51.84
27	78	10	30	0.886	0.156922	3839.87	56.74
27	78	12	30	0.882	0.163122	3983.61	60.20
27	78	14	30	0.883	0.162713	4109.55	63.10
27	78	16	30	0.885	0.126968	4424.97	63.37
30	78	6	30	0.854	0.081558	3494.01	43.56
30	78	8	30	0.866	0.117656	3707.75	51.65
30	78	10	30	0.868	0.142283	3948.51	57.26
30	78	12	30	0.861	0.193856	4090.67	62.34
30	78	14	30	0.864	0.181614	4238.92	66.44
30	78	16	30	0.886	0.135286	4331.03	66.91
24	78	6	20	0.842	0.087007	3051.73	36.45
24	78	8	20	0.846	0.129976	3273.38	41.77
24	78	10	20	0.862	0.138057	3458.09	44.20
24	78	12	20	0.874	0.157939	3595.02	46.44
24	78	14	20	0.861	0.161989	3744.34	49.58
24	78	16	20	0.849	0.146848	3879.15	51.70
24	78	6	25	0.870	0.087249	3221.83	39.91
24	78	8	25	0.862	0.117193	3456.11	45.74
24	78	10	25	0.877	0.132965	3635.20	48.68
24	78	12	25	0.891	0.151936	3770.84	50.87
24	78	14	25	0.887	0.156999	3850.80	53.26
24	78	16	25	0.883	0.141736	3943.42	53.67
24	78	6	35	0.785	0.073870	3491.49	47.73
24	78	8	35	0.793	0.091521	3651.87	59.49
24	78	10	35	0.841	0.125197	3830.72	68.44
24	78	12	35	0.868	0.102371	4021.64	71.17
24	78	14	35	0.894	0.099549	4137.07	73.77
24	78	16	35	0.904	0.096214	4236.78	75.77
24	72	6	30	0.860	0.082017	3162.17	41.43
24	72	8	30	0.868	0.109751	3387.19	47.52
24	72	10	30	0.882	0.124530	3555.81	50.70
24	72	12	30	0.903	0.151873	3682.95	53.16
24	72	14	30	0.905	0.154575	3786.76	54.99
24	72	16	30	0.906	0.151191	3887.88	56.64
24	84	6	30	0.850	0.081156	3371.43	43.45
24	84	8	30	0.863	0.100055	3478.70	50.88
24	84	10	30	0.873	0.127490	3779.49	55.85
24	84	12	30	0.893	0.153872	3927.23	59.07
24	84	14	30	0.893	0.138919	4071.05	61.35
24	84	16	30	0.896	0.125525	4166.97	63.68

5.2. The fitting of key parameters

Yield coefficient (a), initial bending stiffness (S_j) and ultimate bending moment (M_u) are nonlinearly fitted respectively with Eq. (1), and the ultimate rotation (φ_u) is nonlinearly fitted with Eq. (2). The independent variables of the fitted formulas are bolt diameter, bolts' vertical distance, flange thickness and front plate thickness. The values of fitted coefficients are obtained and shown in Tables 6 and 7.

The predicted values are obtained by using the fitted formula, and then scatter diagram (Fig. 18) is plotted with true value as x-axis and the predicted value as y-axis. It can be observed that the points basically fall on the ideal fitting line. It indicates that the fitted formula can accurately calculate the main

parameters of the bilinear model, with 1.30% deviation in the yield coefficient, 2.57% deviation in the initial stiffness, 3.82% deviation in the ultimate moment and 8.65% deviation in the ultimate rotation.

$$y = \frac{(c_1 d + c_2 L_1 + c_3 t_1 + c_4 t_2)^{c_5}}{(dL_1 t_1 t_2)^{c_6}} + c_7 \quad (1)$$

$$\varphi_u = \frac{(c_1 d + c_2 L_1 + c_3 t_1 + c_4 t_2)^{6.8}}{(dL_1 t_1 t_2)^{c_5}} + \frac{(c_6 dt_1 + c_7 t_1 t_2 + c_8 t_2 L_1 + c_9 L_1 d)^3}{(dL_1 t_1 t_2)^{c_5}} + c_{10} \quad (2)$$

Table 6
Specific values of fitting coefficients of a, S_i and M_u

y	c_1	c_2	c_3	c_4	c_5	c_6	c_7
a	+1.466e-5	-1.344e-5	+2.132e-4	-9.195e-5	5.000	-2.128e+0	+8.820e-1
K	+3.145e+2	+3.327e+2	+1.202 e+2	+3.656e+2	1.000	-1.143e-1	+1.124e+7
M_u	-5.423e-3	+4.560e-3	-1.274e-2	+1.424e-2	1.000	-1.310e+0	+3.508e+7

Table 7
Specific values of fitting coefficients of φ_u

c_1	c_2	c_3	c_4	c_5	c_6	c_7	c_8	c_9	c_{10}
+9.181e-3	+1.635e-2	-2.258e-2	+2.347e-2	+5.573e-1	+4.891e-2	-2.993e-2	+8.314e-4	-5.001e-3	+1.276e-1

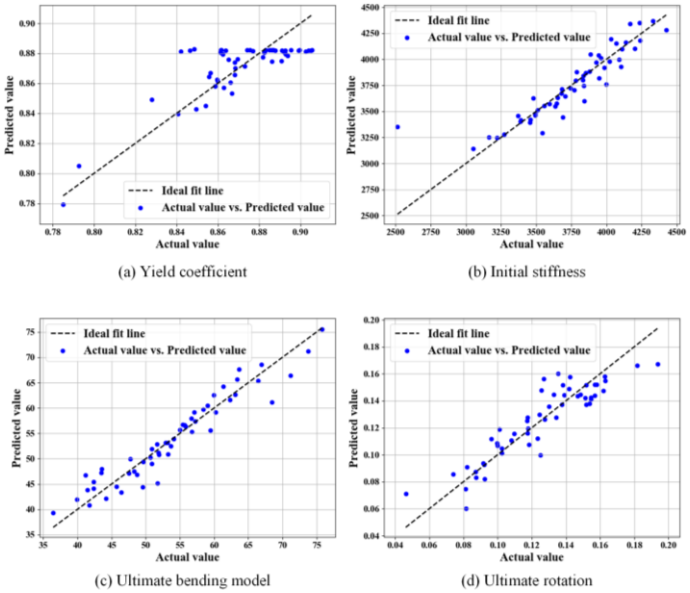

Fig. 18 Scatter diagram of comparison between actual values and predicted values

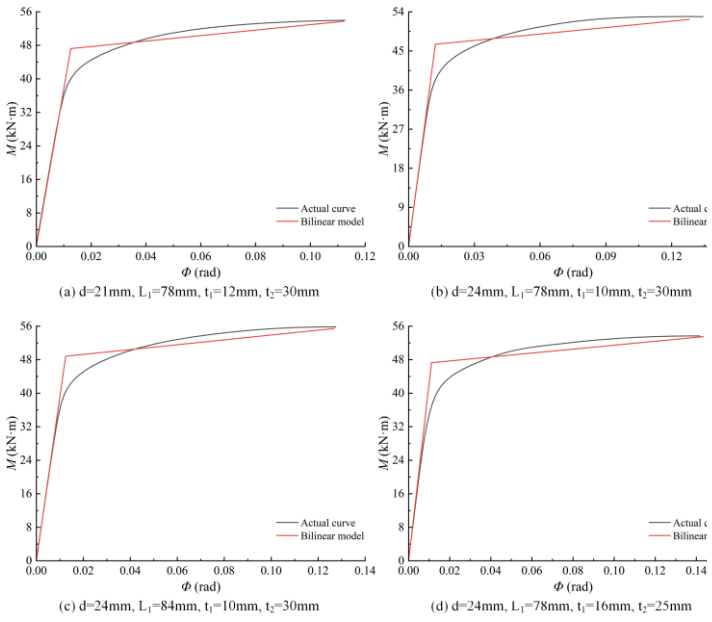

Fig. 19 Comparison of the moment-rotation relationship between bilinear and actual models

5.3. Validation of the fitted bilinear model

In summary, the moment-rotation curve of improved BC joint can be determined according to Eqs. (1)-(2) and Tables 6-7, provided that the bolt diameter, vertical distance between bolts, flange thickness, and front plate thickness of the joint are known. Fig. 19 presents a comparison of moment-rotation curves obtained from the finite element model and the fitted bilinear model. It is evident that the bilinear model accurately represents the stiffness and bending capacity, aligning well with the numerical findings. Hence, it can be inferred that utilizing the bilinear model as a preliminary estimation for predicting the moment-rotation curve of the enhanced BC joint would serve as a reliable reference.

Additionally, it is worth noting that the proposed bilinear model is developed by nonlinear fitting, without any derivation of theory. Thus, its application is constrained by the considered geometrical parameters in Table 5, namely bolt diameter from 21-30mm, bolts' vertical distance from 72-84mm, flange thickness 6-16mm and front plate thickness from 20-35m.

6. Conclusions

The present study proposes a novel structure for the traditional BC joint and conducts a comparison on bending performance between the original and the improved joints. Subsequently, parametric investigation of the improved joint including 66 models is conducted in which different parameters, such as bolt diameter, bolts' vertical distance, flange thickness, front plate thickness and column node thickness, are varied. In addition, the effect of axial force on the bending performance of the joint is also discussed. Finally, the bilinear model of the improved BC joint is established and verified based on FE models. The main conclusions in this paper are summarized as follows.

(1) Compared with traditional BC joint, the improved BC joint exhibits a significant improvement in bending performance including 62.59% increase in initial rotational stiffness, 116.82% increase in initial yield moment, and 87.57% increase in ultimate moment.

(2) The general laws that geometric parameters affect the bending performance are obtained from parametric study.

(i) The ultimate moment of joints increases remarkably with a gradually decreasing rate as the flange thickness increases, while the initial bending stiffness experiences a slight increase. Three different failure modes are observed with the progressive increment in flange thickness: (I) the plastic hinge formation in first half of cone part results the failure of joint; (II) joint failure occurs due to simultaneously yielding among front plate, flanges and bolts; (III) joint failure occurs due to the tensile failure of bolts.

(ii) The ultimate moment of the joint increases as the bolt diameter increases, while a slight decrease occurs in the yield area of the front plate and a relatively significant one for bolts. When $d > 27\text{mm}$, the bolt diameter has little effect on the moment-rotation curve.

(iii) The bending performance of joints can be enhanced by increasing the vertical distance between bolts, and a gradual increase in the vertical distance between bolts leads to a stable improvement in the ultimate moment of joints and a reduction in bolt stress.

(iv) As the thickness of the front plate increases, there is a corresponding increase in the ultimate moment of joints, accompanied by an increase in stress and deformation of flanges. Except for joints with a flange thickness of 16mm, the failure mode remains consistent for joints with a front plate thickness of

30mm: both flanges form plastic hinges, resulting in the failure of joint.

(v) The moment-rotation curve remains little change when the thickness of the column node exceeds 40mm. When the thickness is less than 40mm, flanges with thicknesses over 10mm slightly affect the bending performance of the joint, and the failure modes of such joints are that the entire area of the column node yields. Therefore, it is recommended to have a thickness greater than 40mm for the column node.

(3) When axial compression is small, it exhibits positive effect on the bending performance of improved BC joint; however, the axial tension demonstrates negative influence on the bending performance consistently.

(4) A bilinear model is developed by incorporating parameters including bolt diameter, bolts' vertical distance, flange thickness, and front plate thickness. Comparative study demonstrates that the model can accurately predict the bending behavior of the improved BC joint.

Acknowledgements

This work was supported by National Natural Science Foundation of China (No.51408490), Natural Science Basic Research Program of Shaanxi (2022JM-234, 2023-JC-YB-363), Training Programs of Innovation and Entrepreneurship for Undergraduates (202310712067, 202410712019), are gratefully appreciated.

References

[1] Huihuan Ma, Shan Ren, Feng Fan. Parametric study and analytical characterization of the bolt-column (BC) joint for single-layer reticulated structures [J]. Engineering Structures, 2016, 123: 108-123. (DOI: 10.1016/j.engstruct.2016.05.037)

[2] Huihuan Ma, Shan Ren, Feng Fan. Experimental and numerical research on a new semi-rigid joint for single-layer reticulated structures [J]. Engineering Structures, 2016, 126: 725-738. (DOI: 10.1016/j. engstruct.2016.08.028.)

[3] Feng Fen, Huihuan Ma, Xin Jiang. Optimization of spatial semi-rigid C-joint and experimental study on its rotational resistance [J]. Journal of Building Structures, 2016, 37(03): 134-140. (DOI: 10.14006/j.jzjgxb.2016.03.016) (in Chinese)

[4] Qinghua Han, Yiming Liu, Ying xu. Stiffness characteristics of joints and influence on the stability of single-layer latticed domes [J]. Thin-Walled Structures, 2016, 107: 514-525. (DOI: 10.1016/j.tws. 2016.07.013)

[5] Ren-Zhang Yan, Chang-Long Zhang, Shuai Wang, *et al*. Distribution of residual stress in the sphere-pipe connection welds of welded hollow spherical joints [J]. Advanced Steel Construction, 2023, 19(03): 262-272. (DOI: 10.18057/IJASC.2023.19.3.7)

[6] Waleed Mashrah, Zhi-Hua Chen, Hong-Bo Liu, *et al*. Experimental, numerical, and theoretical study on static behaviour of novel steel dovetail joint subjected to axial tension load [J]. Advanced Steel Construction, 2022, 18(01): 453-464. (DOI: 10.18057/ IJASC.2022.18.1.4)

[7] Feng Fan, Huihuan Ma, Gengbo Chen et al. Experimental study of semi-rigid joint systems subjected to bending with and without axial force [J]. Journal of Constructional Steel Research, 2012, 68: 126-137. (DOI: 10.1016/j.jcsr.2011.07.020)

[8] Feng Fan, Huihuan Ma, Shizhao Shen. Numerical simulation and experimental study on mechanical characters of bolt-boll joint system [J]. Engineering Mechanics, 2009, 26(12): 92-99. (DOI: 10.1109/CLEOE-EQEC.2009.5194697) (in Chinese)

[9] Xiaochen Yu, Huijun Li, Xu Chen et al. Mechanical properties of bolt-ball joints and establishment of moment-rotation relation formula [J]. Progress in Building Structures, 2022, 24(04): 57-65. (DOI: 10.13849/j.issn.1006-6578.2022.02.056) (in Chinese)

[10] Su-duo Xue, Si-yao Li, Xiong-yan Li, *et al*. Behaviour and mathematical model for semi-rigid threaded-sleeve connection [J]. Advanced Steel Construction, 2019, 15(02): 123-128. (DOI: 10.18057/ IJASC.2019.15.2.1)

[11] Hui-Huan Ma, Yue-Yang Ma, Feng Fan, *et al*. Seismic performance of single-layer spherical reticulated shells considering joint stiffness and bearing capacity [J]. Advanced Steel Construction, 2022, 18(02): 604-616. (DOI: 10.18057/IJASC.2022.18.2.9)

[12] Chen Shan. Analysis of Hub-Shape inlay joint and its influence on the stability of single-layer lattice domes [D]. Tianjin: Tianjing University, 2010. (DOI: 10.7666/d.y1925692) (in Chinese)

[13] Qinghua Han, Yiming Liu, Jinyuan Zhang et al. Mechanical behaviors of the Assembled Hub (AH) joints subjected to bending moment [J]. Journal of Constructional Steel Research, 2017, 138: 806-822. (DOI: 10.1016/j.jcsr.2017.08.026)

[14] Xiaolei Zhang, Huijun Li, Xiaochen Yu et al. Research on stiffness and bilinear model of hub-shape inlay joints [J]. Spatial Structures, 2022, 28(02): 56-86. (DOI: 10.13849/j.issn.1006-6578. 2022. 02. 056) (in Chinese)

[15] Tudor Golea, Jean-Pierre Jaspart, Jean-François Demonceau. Characterisation of the behaviour of beam-to-column steel joints up to failure [J]. Advanced Steel Construction, 2022, 18(03): 679-686. (DOI: 10.18057/IJASC.2022.18.3.5)

[16] Huihuan Ma, Lingwei Yu, Feng Fan et al. Mechanical performance of an improved semi-rigid joint system under bending and axial forces for aluminum single-layer reticulated shells [J]. Thin-Walled Structures, 2019, 142: 322-339. (DOI: 10.1016/j.tws.2019.05.003)

[17] Huihuan Ma, Yuqi Jiang, Chengrui Li et al. Performance analysis and comparison study of two aluminum alloy joint systems under out-of-plane and in-plane loading. An experimental and numerical investigation [J]. Engineering Structures, 2020, 214(2): 110643. (DOI: 10.1016/j.engstruct.2020. 110643)

[18] Huihuan Ma, Lingwei Yu, Wei Wang et al. Static stability of aluminium single-layer elliptical parabolic latticed shell with semi-rigid joints [J]. Engineering Mechanics, 2017, 34(11): 158-166. (DOI: 10.6052/j.issn.1000-4750.2016.07.0535) (in Chinese)

[19] Ruoqing Fan, Fengcheng Liu, Guirong Yan et al. Mechanical behavior of Ring-sleeve joints of single-layer reticulated shells [J]. Journal of Constructional Steel Research, 2017, 128: 601-610. (DOI: 10.1016/j.jcsr.2016.09.023)

[20] Hui-Huan Ma, Chen-Yang Zhao, Yu-Qi Jiang, *et al*. Rotational resistance test of a new aluminum alloy penetrating (aap) joint system [J]. Advanced Steel Construction, 2023, 19(03): 121-129. (DOI: 10.18057/IJASC.2023.19.2.4)

[21] G. De Matteis, A. Mandara, F.M. Mazzolani. T-stub aluminium joints: influence of behavioural parameters [J]. Computers and Structures, 2000, 78(1-3): 311-327. (DOI: 10.1016/S0045-7949 (00)00081-X)

[22] Gianfranco De Matteis, Muhammad Tayyab Naqash, Giuseppe Brando. Effective length of aluminium T-stub connections by parametric analysis [J]. Engineering Structures, 2012, 41: 548-561. (DOI: 10.1016/j.engstruct.2012.03.052)

[23] Chenaghlou M R, Nooshin H. Axial force-bending moment interaction in a jointing system part I: (Experimental study) [J]. Journal of Constructional Steel Research, 2015, 113: 261-276. (DOI: 10.1016/j.jcsr.2015.06.011)

[24] Chenaghlou M R, Nooshin H. Axial force-bending moment interaction in a jointing system part II: Analytical study [J]. Journal of Constructional Steel Research, 2015, 113: 277-285. (DOI: 10.1016/j.jcsr.2015.06.010)

[25] Guo X, Xiong Z, Luo Y, *et al*. Experimental investigation on the semi-rigid behaviour of aluminium alloy gusset joints [J]. Thin-Walled Structures, 2015, 87: 30-40. (DOI: 10.1016/j.tws. 2014.11.001)

[26] Đorđe, Đuričić, Srđa, *et al*. Experimental, theoretical and numerical analysis of K-joint made of CHS aluminium profiles [J]. Thin Walled Structures, 2017, 119: 58-71. (DOI: 10.1016/j.tws.2017. 05.016)